Nano Energy 47 (2018) 309–315

Contents lists available at ScienceDirect

Nano Energy

journal homepage: www.elsevier.com/locate/nanoen

Full paper

Robust and conductive Magnéli Phase Ti_4O_7 decorated on 3D-nanoflower NiRu-LDH as high-performance oxygen reduction electrocatalyst

Kassa Belay Ibrahim[a], Wei-Nien Su[a,*], Meng-Che Tsai[b], Soressa Abera Chala[b], Amaha Woldu Kahsay[b], Min-Hsin Yeh[b], Hung-Ming Chen[b], Alemayehu Dubale Duma[a], Hongjie Dai[c], Bing-Joe Hwang[b,d,**]

[a] Nano-electrochemistry Laboratory, Graduate Institute of Applied Science and Technology, National Taiwan University of Science and Technology, Taipei 106, Taiwan
[b] Nano-electrochemistry Laboratory, Department of Chemical Engineering, National Taiwan University of Science and Technology, Taipei 106, Taiwan
[c] Department of Chemistry, Stanford University, Stanford, CA 94305-4401, USA
[d] National Synchrotron Radiation Research Center, Hsin-Chu, Taiwan

ARTICLE INFO

Keywords:
Layered double hydroxides
Oxygen reduction reaction
3D nano-flower
Agglomeration
Substoichiometric TiO_2

ABSTRACT

Escalating both electrochemically active and stable materials at a time is an important challenge in the field of catalysis till to date. Carbon as a pillar material has been used for long time due to its intrinsic properties like high conductivity and large surface area that can increase activity of electrocatalyst. However, severe drop in activity due to carbon corrosion is the main challenge. Here, we introduce robust, conductive and stable Magnéli phase Ti_4O_7 nano-pillar in to flower like nickel ruthenium-layered double hydroxide (3D-FL-NiRu-LDH/ Ti_4O_7) through an easy in situ growth approach for the first time. The decoration of Magnéli phase Ti_4O_7 not only significantly improves the activity but also stability of LDH nanosheet catalyst. The as-synthesized materials retain 98% of the activity after 45 h which surpasses all the reported LDH catalysts for oxygen reduction reaction under alkaline media. The key roles of Ti_4O_7 are to provide the effective charge transfer networks of LDH catalyst and prevent agglomeration of LDH catalysts though strongly coupled interactions evidenced by X-ray photoelectron spectroscopy (XPS). Therefore, the developed catalyst demonstrates promising conductivity, together with durability. The reported approach of introducing a robust and conductive pillar coupled with LDH catalysts provides a novel pathway for developing a highly efficient and durable electrocatalyst.

1. Introduction

The modern society is actively seeking for a new means of generating clean, sustainable, and renewable energy to meet the ever-increasing energy demand while grappling with the alarming concerns of global warming and depletion of natural resources. One of the challenges of a working fuel cell is that the cathode catalyst must be chemically active enough to activate O_2 but should remain sufficiently noble to release the oxygen species in the form of H_2O [1]. However, the sluggish kinetics of oxygen reduction reaction (ORR) to water in cathode side, corrosion of carbon material and high cost and instability of cathodic Pt, limits the commercial application of existing fuel cell technology.

Recently, LDH materials attract a great deal of attention in the fields of energy conversion and storage [2,3], electrocatalysis [4], and sensor [5], due to having promising catalytic activity, selectivity, and stability. These unique properties of LDHs afford superior electrocatalytic performance [6]. As an attractive catalyst material, LDHs possess brucite-like layers that have an abundance of basic sites, thus allowing LDHs as a heterogeneous solid base catalyst. The metal cations that form brucite-like layers are uniformly distributed without segregation, and when one of them is a catalytically active transition metal, this can lead to high catalytic activity and selectivity [7]. An assortment of dual-metal NiFe-LDH [8,9], NiCo-LDH [10], CoMn-LDH [11], and CoFe-LDH [12], CoFe-LDH [13], FeNi-LDH [14], NiMn-LDH/CNT [15], NiTi-LDH [16], and O-NiCoFe-LDH [17], have been investigated for the role of an efficient oxygen evolution reaction (OER) electrocatalyst. However, there is still limited report on using LDHs as ORR electrocatalyst materials [18,19]. Lately, a ternary (NiCoFe) LDH [17] and $Ni_2Co^{III}Fe$-LDH/N-GO [20] are reported as a high-performance bifunctional oxygen electrode catalyst. But poor conductivity hinders the competition of LDHs with other catalysts as best candidate of ORR electrocatalysts [21].

* Corresponding author.
** Correspondence to: Nano-electrochemistry Laboratory, Department of Chemical Engineering, National Taiwan University of Science and Technology, 43 Keelung Road, Section 4, Taipei 106, Taiwan.
E-mail addresses: wsu@mail.ntust.edu.tw (W.-N. Su), bjh@mail.ntust.edu.tw (B.-J. Hwang).

https://doi.org/10.1016/j.nanoen.2018.03.017
Received 6 January 2018; Accepted 5 March 2018
Available online 07 March 2018

Consequently, LDHs have been blended with carbon materials having more π sites (e.g., graphene [22], nanotube array [22], and carbon nanotube [9]) to facilitate charge transfer, minimize particle agglomeration, and improve electronic conductivity. However, thermodynamically instability at potentials > 0.9 V of carbon results to a permanent carbon loss, extremely weak Van-der-Waals force interactions with supported catalysts, a serious catalyst detachment, and, in the extreme, a structural collapse of the electrode are the main challenges till to date. To overcome such challenges of carbon based supports, interesting approach so-called interaction between metals and oxide supports (metal-support interactions) are being investigated [23–25].

In this regard, TiO_2 is feasible alternative, especially when one considers the cost, abundance of its main precursor, structural and chemical stability under harsh environment, the ability to form strong interactions with metal oxide nanoparticles [26], that could avoid agglomeration, disperse metal atoms in the clusters, and produce an electronic effect on metal oxide nanocatalysts consistently, modify the catalytic property of catalysts. However, still the intrinsically poor electrical conductivity limits the use of TiO_2 to support, decorate and use as pillar for electrocatalyst. Therefore, for metal oxides to be used as fuel cell catalyst supports they should have good conductivity, a high surface area, high stability and extended durability. Therefore, researchers have try to improve conductivity of TiO_2 through introducing an appropriate donor dopants [25], and reduction at high temperature annealing to form oxygen vacancy although controlling particle growth is the main challenge in this method [27]. During high temperature reduction of TiO_2, different Magnéli phase oxides as described with the general formula Ti_nO_{2n-1}, $3 < n < 10$ are formed [23]. Among them, Ti_4O_7 is the most conductive (having theoretical conductivity of, 10^3 S/cm) metal oxide based pillar. In addition to its comparable conductivity with carbon materials, it also exhibits several unique properties like excellent resistance to electrochemical oxidation, higher corrosion resistance, and robustness in aggressive (acidic and basic) conditions.

Fundamentally, the core objective of this work is to address the major challenge like poor conductivity, limited surface area and short term durability that affects the use of LDHs as electrocatalysts. Our approach involves integrating LDH with a highly conductive and corrosion-resistant metal oxide (Magnéli phase Ti_4O_7), and morphologically engineering the material into a 3D hierarchical structure to improve conductivity, durability and to create more accessible active site for the electrolyte. Herein, we report fabricate 3D hierarchical flower-like NiRu-LDHs using sodium dodecyl sulfate (SDS) as a template to control material morphology; and urea as a source of intercalated CO_3^{2-} anions and also to adjust the pH value of the solution (as illustrated in Equation (S1)). The overall fabrication process of 3D-FL-NiRu-LDH/Ti_4O_7 is shown in Scheme 1. The hierarchical structure of the obtained material enables convenient charge transfer, along with a strong electronic coupling. Morphological engineering (which increases surface area) and the use of a highly conductive and robust Ti_4O_7 pillar has expected to facilitate charge separation and electron transfer at a mean time it prevents particle agglomeration through forming strong interaction with LDH. The synthesis procedure is illustrated in Scheme S1. To the best of our knowledge; this is the first study to report an LDH decorated by a high-temperature-reduced Ti_4O_7 as an ORR electrocatalyst.

2. Experimental methods

2.1. Preparation of Ti_4O_7 as a catalyst support

Magnéli-phase Ti_4O_7 was prepared via a modified procedure involving the reduction of stoichiometric anatase TiO_2 powder at 1000 °C under H_2 flow (Proxair,99.99%) at a rate of 50 cm^3/min for 4 h [28]. Under vigorous stirring, 0.3 g of TiO_2mixedwith 25.8 mL of ethanol and 10 mL of 50 mM tetraethylorthosilicate (TEOS. 35% $NH_3$was added to maintained pH of the solution followed by deionized (DI) water). The solution was then stirred for 14 h at room temperature. The solution was subsequently centrifuged, and the precipitate was repeatedly washed with EtOH and DI water until the pH = 7. The solid was dried overnight in a vacuum oven at 80 °C. Thereafter, the powder was transferred to an L-tube and reduced with pure H_2 at 1000 °C for 4 h. Finally, the Ti_4O_7 powder was etched with 2% hydrogen fluoride (HF) to remove SiO_2.

$$2TiOH + [Si(OCH_3)_3]_2HN \rightarrow 2TiOSi(CH_3)_3 + NH_3$$

The overall synthesis is shown in Scheme S2.

2.2. Synthesis of 3D nanoflower-like NiRu-LDH

(3D-FL-NiRu-LDH): 3D-FL-NiRu-LDH was synthesized using the following optimized procedure. A total of 3.2 mmol of Ni^{2+} and Ru^{3+}(i.e., 2.4 mmol of $(Ni(NO_3)_2{\cdot}6H_2O$ and 0.8 mmol of Ru(NO)$(NO_3)_3$), 0.6 mmol of sodium dodecyl sulfate (as template), and 1.25 g of urea were dissolved in 12 mL of DI water and 38 mL of ethylene glycol to give a 50-mL mixture solution. The solution was stirred continuously for 30 min at room temperature, followed by 10 min of ultrasonication. The mixture was then transferred to a Teflon-lined stainless steel autoclave thrice, and subsequently heated in an oven at 150 °C for 12 h. Finally, the resulting 3D-FL-NiRu-LDH was washed thrice with DI water and ethanol thoroughly, and dried overnight under vacuum at 80 °C [29]. The same procedure but in the absence of sodium dodecyl sulfate (SDS) resulted in NiRu-LDH, which was used for comparative analysis.

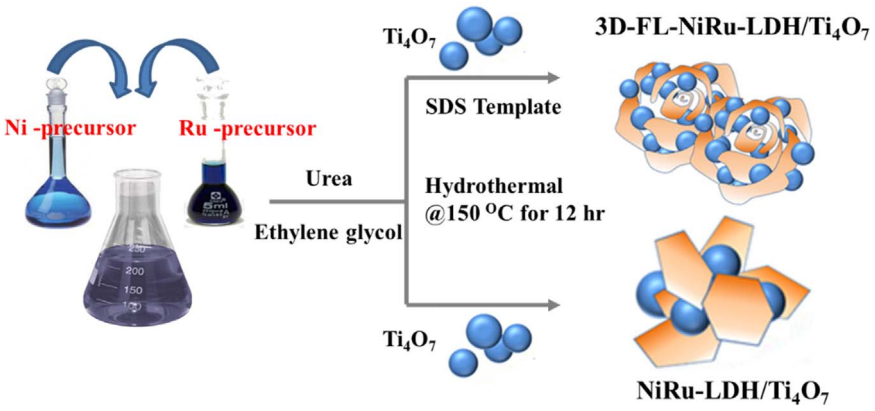

Scheme 1. Schematic representation of the synthesis of 3D-FL-NiRu-LDH/Ti_4O_7.

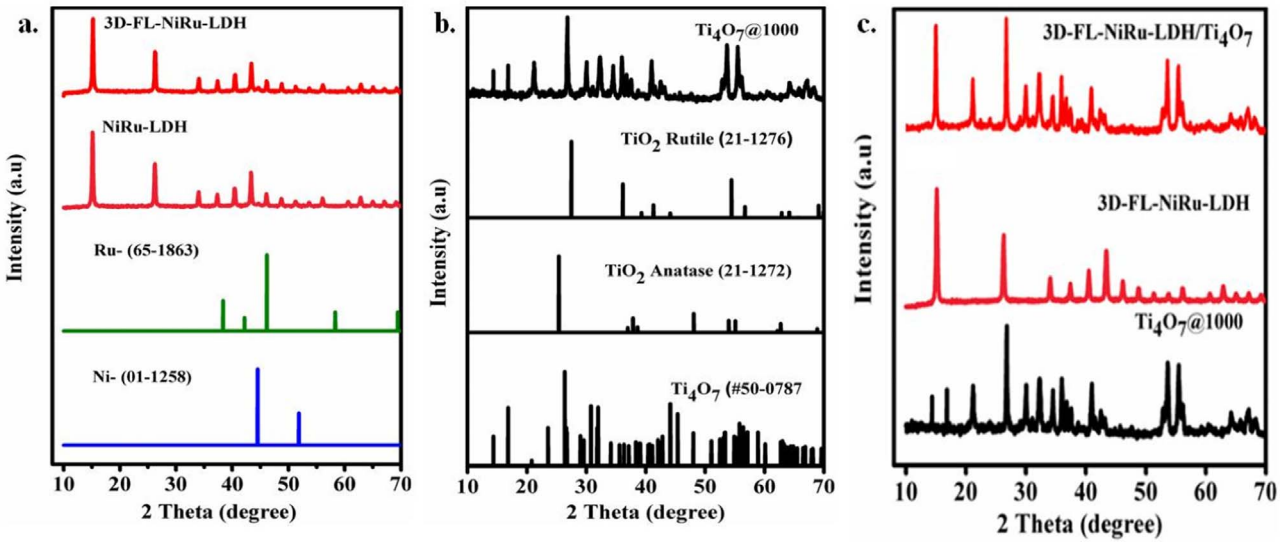

Fig. 1. XRD patterns for the (a) 3D-FL-NiRu-LDH (b) as prepared Ti_4O_7 support and (c) 3D-FL-NiRu-LDH/Ti_4O_7.

Table 1
Summary of specific surface area and conductivity of LDHs and TiO_2 derived samples.

Sample	Specific surface area ($m^2\ g^{-1}$)	Conductivity ($S\ cm^{-1}$)
Commercial TiO_2	230.0	3.6×10^{-4}
Ti_4O_7@1000	12.0	730
NiRu-LDH	43.8	2.8×10^{-3}
3D-NiRu-LDH	108.5	2.3×10^{-2}
3D-NiRu-LDH/Ti_4O_7	112.4	628

2.3. Synthesis of 3D-FL-NiRu-LDH/Ti_4O_7

3D-FL-NiRu-LDH and NiRu-LDH were prepared using the aforementioned procedure, with and without sodium dodecyl sulfate as a template. A total of 0.1 g of Ti_4O_7 (1:1 M ratio of LDH to Support) was dispersed in the LDH solution and stirred continuously for 30 min at room temperature, followed by 10 min of ultrasonication. The mixture was then transferred in to a Teflon-lined stainless steel autoclave and heated in an oven at 150 °C for 12 h. Finally, the resulting 3D-FL-NiRu-LDH/Ti_4O_7 was washed thrice with water and anhydrous ethanol thoroughly, and dried overnight in a vacuum oven at 80 °C [30]. NiRu-LDH was prepared using the same protocol used to synthesize 3D-FL-NiRu-LDH except SDS template.

2.4. Electrochemical measurements

Performance of the ORR catalyst was measured with a three-electrode system in a 0.1 M KOH solution using graphite and Ag/AgCl as counter and reference electrode respectively through purged with high-purity argon and oxygen for about 30 min prior to each measurement at room temperature. The working electrode was prepared through, 14 mg of catalyst and 50 μL of Nafion solution were added in to a mixture of isopropanol (700 μL) and de-ionized water (250 μL), and sonicate for 50 min to form a homogeneous catalyst slurry. Then, 14 μL of the ink was drop cast on to a glassy carbon to give a catalyst loading of ~ 0.12 mg cm^{-2}, and dried in air. We report all potentials against the RHE potential. Cyclic voltammetry and ORR polarization curves were measured through a continuous flow of O_2 at a scan rate of 50 mV s^{-1} and 1 mV s^{-1}, respectively. The practical application of the ORR catalysts was also further investigated by testing the stability of the as synthesized material on Ni-foam. The stability of the material was tested by loading (20 μL of ink) to 1 cm *1 cm area Ni-foam and at 0.7 V for about 45 h under 1 M KOH solution.

2.5. Physical characterizations

Morphological and structural characterizations were performed using transmission electron microscopy (TEM) with an FEI Tecnai G2 F20 S-Twin electron microscope, operating at 200 kV. Meanwhile, scanning electron microscopy (SEM) images and energy dispersive X-ray (EDX) analysis was conducted with an FEI Quanta 200 scanning electron microscope, operating at an acceleration voltage of 20 kV. Crystalline structure was measured via X-ray diffraction analysis using a Bruker D2 Phaser XRD machine, equipped with a Cu-Kα irradiation photon source (λ = 1.5406 Å, Ni filter, 40 kV, and 100 mA). All samples were analyzed at room temperature in the 2θ range of 10–80°, with a scanning speed of 0.1° s^{-1} and 0.05°/step. Thermal stability was tested using thermogravimetric analysis (TGA), performed on a Perkin-Elmer TGA-7 Thermo Analyzer under air flow at a rate of 10 °C min^{-1}. Specific surface area and pore size were measured using Brunauer–Emmet–Teller analysis, as determined by nitrogen adsorption-desorption isotherms on Quanta chrome Nova Win instrument at 200 °C. X-ray photoelectron spectroscopy was performed using a wide-range beamline (BL24A) at the National Synchrotron Radiation Research Center (NSRRC) in Taiwan. All reported binding energies were corrected using the signal for the carbon peak (C 1s) at 284.5 eV.

3. Results and discussion

3.1. Morphological and structural characterizations

The XRD pattern of bare 3D-FL-NiRu-LDH, Ti_4O_7 and 3D-FL-NiRu-LDH/Ti_4O_7 hybrid are presented in Fig. 1. As shown in Fig. 1**a,** the XRD pattern of bare 3D-FL-NiRu-LDH showed an obvious layered structure with a basal space of 0.78 nm. In addition, the characteristic reflections of (003), (006), (101), (120), (009), (015), (018), (0111), (110), and (113) can be indexed to a typical hydrotalcite-like structure that is attributed to the lattice planes of 3D-FL-NiRu-LDH and designated with the $R\bar{3}m$ space group. The rhombohedral LDH phase with a brucite-like sheet interlayer spacing (d_{003}) of 0.78 nm is in accordance with the reported value for NiFe-LDH with CO_3^{2-} ions as interlayer anion [17]. Moreover, the (102), (120), (122), (104), (200), (104), (120), (024), and (326) reflections peaks of Ti_4O_7 (Fig. 1**b, c)** was observed in 3D-FL-NiRu-LDH/Ti_4O_7 hybrid, confirms the formation of 3D-FL-NiRu-LDH/Ti_4O_7 composite.

The vibration dynamics of Ni/Ru-O, Ni-Ru and Ni-O-Ru was investigated using Raman spectroscopy. The prominent absorption peaks

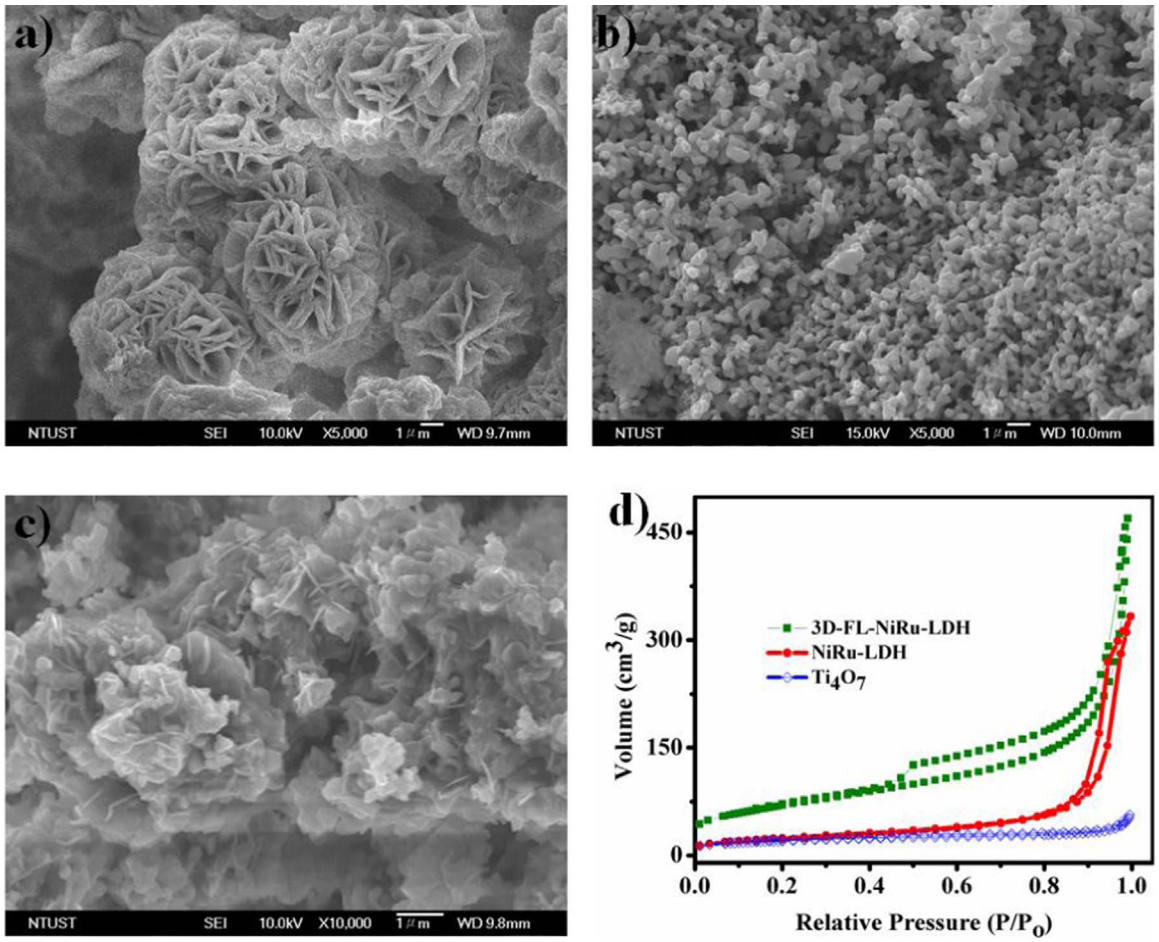

Fig. 2. SEM images of (a) 3D-FL-NiRu-LDH, (b) Ti_4O_7, (c) 3D-FL-NiRu-LDH/Ti_4O_7,(d) N_2 adsorption-desorption isotherms of NiRu-LDH, Ti_4O_7,and 3D-FL-NiRu-LDH.

for 3D-FL-NiRu-LDH at 547 and 700 cm^{-1} (Fig. S2a) corresponds to Ni^{2+}/Fe^{3+} -O-Ni^{2+}/Ru^{3+} and Ru^{3+}-O-Ru^{3+} linkage in the structural units of $M(OH)_2$ (M = Ni, Ru) [20]. At a mean time, an intense prominent peak at around 1063 $cm^{-1}$is corresponds to Ni-O or Ru-O bands that are oxygen active species with a hydroxide nature [31–34]. The FT-IR spectra (Fig. S3a,**b**) of pure LDH show a sharp peak at 1640 cm^{-1}, which is attributed to the stretching vibration of the interlayer CO_3^{2-} ion that supports the XRD peak (003) that corresponds to that CO_3^{2-} ions and water molecules occupied the interlayer galleries of the LDH [35,36]. The bands in the low frequency region at around 700 cm^{-1} are related with M-O-M lattice vibrations i.e. Ni–O, Ru–O and Ni–O–Ru, of the layer cations of LDH [35,36]. The shoulder band around 3500 cm^{-1} could be attributed to the stretching vibration of the O–H group from both the hydroxide layers and interlayer water [37]. The broadness of the O–H peak may be due to the lower electron density of the O–H groups bonded to Ru^{3+} cations, because of the larger polarizing effect of the trivalent cation [38]. The results of FT-IR confirm the formation of NiRu- LDH, which are in good agreement with the results obtained in Raman (Fig. S2a). Raman peaks measurement (Fig. S2b) has also performed in order to confirm the formation of Ti_4O_7. The conductivity of the as-synthesized samples was measured using a four-point probe method and it was found comparable to that of previously reported materials as summarized in Table 1.

In order to inspect the microstructure and morphology of the as-prepared samples, the product was characterized by SEM as presented in Fig. 2. The observed images in Fig. 2**a-c** showed the uniform dispersion of flower-like structure and formation of an entangled network due to decoration of pristine 3D-FL-NiRu-LDH material by Ti_4O_7. The formation of an entangled network between LDH and pillar material together with 3D hierarchical prevents agglomeration of composite material. Thus, it was benefits to the electronic transmission, ion diffusion and to have an extended durability. Moreover, the TEM (Fig. S4a, **b**), EDX (Fig. S5**a-c**) and elemental maps of Ni, Ru and O confirm all elements were uniformly distributed in the NiRu-LDH/ Ti_4O_7 composite.

Surface area of the as-prepared materials was characterized using Brunauer–Emmet–Teller (BET) analysis. Hence, surface area is the most important morphological factor for electrocatalysts, and it is typically measured using nitrogen adsorption-desorption isotherms. As shown in Fig. 2**d** the specific surface area of morphologically engineered 3D-FL-NiRu-LDH (108.5 m^2 g^{-1}) is higher than that of original NiRu-LDH (43.8 m^2 g^{-1}), and Magnéli phase Ti_4O_7 (12.0 m^2 g^{-1}) which have a significant contribution to the superb catalytic activity. The morphological engineering and hybridizing 3D-FL-NiRu-LDH with Ti_4O_7 exposes more active site to the electrolyte and decreasing agglomeration of composite material (that has surface area of 3D-FL-NiRu-LDH/Ti_4O_7 (112.4 m^2 g^{-1}).

In order to better understand the surface chemical states of the as-synthesized LDH, X-ray photoelectron spectroscopy (XPS) measurement was conducted. Subsequently, the formed 3D-FL-NiRu-LDH/Ti_4O_7 with Ni–O–Ti and Ni–O–Ru bonds may adjust the electron density of the metal sites. As revealed in Fig. 3**a** the characteristic peaks of Ni shows BE shift toward lower binding energy, indicates that the electron-rich structure of Ni was induced by the delocalized of electrons near the Ru and Ti atoms. In the case of Ru, the C 1s peak (reference) overlaps with the signals of Ru $3d_{3/2}$ and occasionally, the same thing is observed with the Ru $3d_{5/2}$ peak. For this mater, Ru 3p is preferred for analysis [39]. Due to the preoxidation of Ru^{2+} to Ru^{3+}, the BE of Ru ion

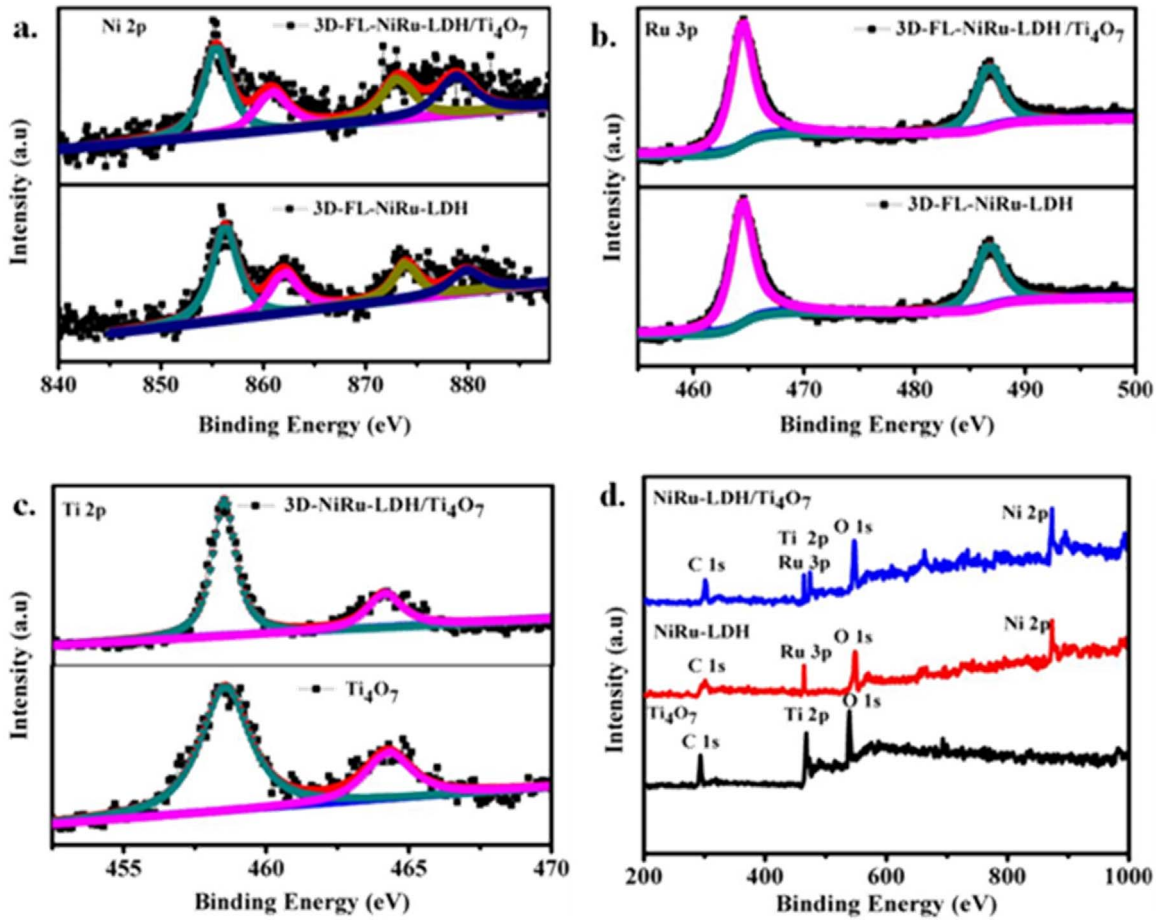

Fig. 3. XPS spectra of (a) Ni, (b) Ru, and (c) Ti sites in 3D-FL-NiRu and 3D-FL-NiRu-LDH/Ti_4O_7 (d) the respective wide-range XPS spectra.

(Fig. 3**b)** shows shift to a higher position, indicates the existence of a high valence state of Ru^{3+}. Similarly, positive BE shift in Ti_4O_7 (Fig. 3**c**) is also observed after coupling it with LDH. Such shifts suggest that the chemical coupling interaction occurs between Ti_4O_7 and 3D-FL-NiRu-LDH [40–42]. In general, the BE shift in the Ni and Ru core level of electron is mainly due to changes in the electronic properties of LDH induced by: (i) the charge transfer from the Ti_4O_7 to LDH and (ii) changes in the lattice parameter due to strong interaction between the oxide support and catalyst. Based on the above XPS analysis, it was clear that a certain synergistic interaction in the electronic structure between the oxide and LDH (electron donation from the oxide to LDH) in the 3D-FL-NiRu-LDH/Ti_4O_7 composites was likely created.

The wide-range XPS spectra (Fig. 3**d**) provides an interestingly the existence of chemical elements of Ni, Ru, Ti, and O in the hybrid material based on their respective binding energy. The O1s peak that appeared in all the spectra could potentially attributed either an oxygen-containing species or adsorbed oxygen atom on the metal surfaces.

3.2. ORR performance of 3D-FL-NiRu-LDH/Ti_4O_7

The cyclic voltammetry (CV) behavior of the as-prepared electrocatalysts was studied using a three-electrode system with glassy carbon electrodes immersed in 0.1 M KOH as the electrolyte. The CV curves for NiRu-LDH/Ti_4O_7 and 3D-FL-NiRu-LDH/Ti_4O_7 (Fig. 4**a**) were obtained in O_2-and Ar-saturated electrolytes and all CV measurements were taken after 50 cycles at a scan rate of 50 mV s^{-1}. Fig. 4**a** provides an information that the absence of obvious cathodic peak under Ar saturation and the presence of characteristic oxygen reduction signals (cathodic peak) at 0.65 and 0.7 V (versus reversible hydrogen electrode (RHE)) in O_2-saturated electrolyte for NiRu-LDH/Ti_4O_7 and 3D-FL-NiRu-LDH/Ti_4O_7, respectively. The polarization curve in Fig. 4**b** shows a typical ORR onset potential of ~ 0.85 V and a half wave potential of ~ 0.68 V for 3D-FL-NiRu-LDH/Ti_4O_7, that is by far the best performance measured to date when compared to LDH materials reported previously [17]. Meanwhile, the respective limiting current for 3D-FL-NiRu-LDH/Ti_4O_7 found is 5.5 mA cm^{-2}, which is comparable to that of 20% Pt/C (6 mA cm^{-2}).

To reveal the electrochemical kinetics and electron transfer mechanism of 3D-FL-NiRu-LDH/Ti_4O_7, Koutecky-Levich (K-L) plots derived from a rotating disk electrode at rotation rates of 400–2025 rpm were used (Fig. 4**c, d**). Based on this, the good linearity and near parallelism properties of the K-L plots suggests that first-order reaction kinetics with respect to the concentration of dissolved O_2, with similar electron transfer numbers for ORR at different potentials. Fig. 4**d** and Fig. S6b provides that 3D-FL-NiRu-LDH/Ti_4O_7 and NiRu-LDH/Ti_4O_7 have ~ 3.94 and ~ 3.4 electron transfer number (n) in the potential range of 0.25–0.45 V respectively. The dominant selectivity of the four-electron reduction pathway shows that ORR is an ideal four-electron reaction for converting oxygen to OH^-. The smaller Tafel slope in 3D-FL-NiRu-LDH/Ti_4O_7 (~ 58 mV dec^{-1}, Fig. S6d) compared to NiRu-LDH/Ti_4O_7 (~ 64 mV dec^{-1}, Fig. S6c) indicates faster reaction kinetics and relatively smaller over potential, which is similar to the well-known volcano plots. Therefore, the nearly identical Tafel slopes of NiRu-LDH and 3D-FL-NiRu-LDH demonstrated that both types of materials utilize the same four-electron ORR pathway.

Although the as- synthesized 3D-FL-NiRu-LDH/Ti_4O_7 catalyst shows an inferior activity compared to 20% Pt/C (Fig. S6e) but it has a superior catalytic activity relative to previously reported LDH-based catalysts as summarized in Table 2. Furthermore, 3D-FL-NiRu-LDH/Ti_4O_7 exhibits remarkable and superior durability over both 20% Pt/C and

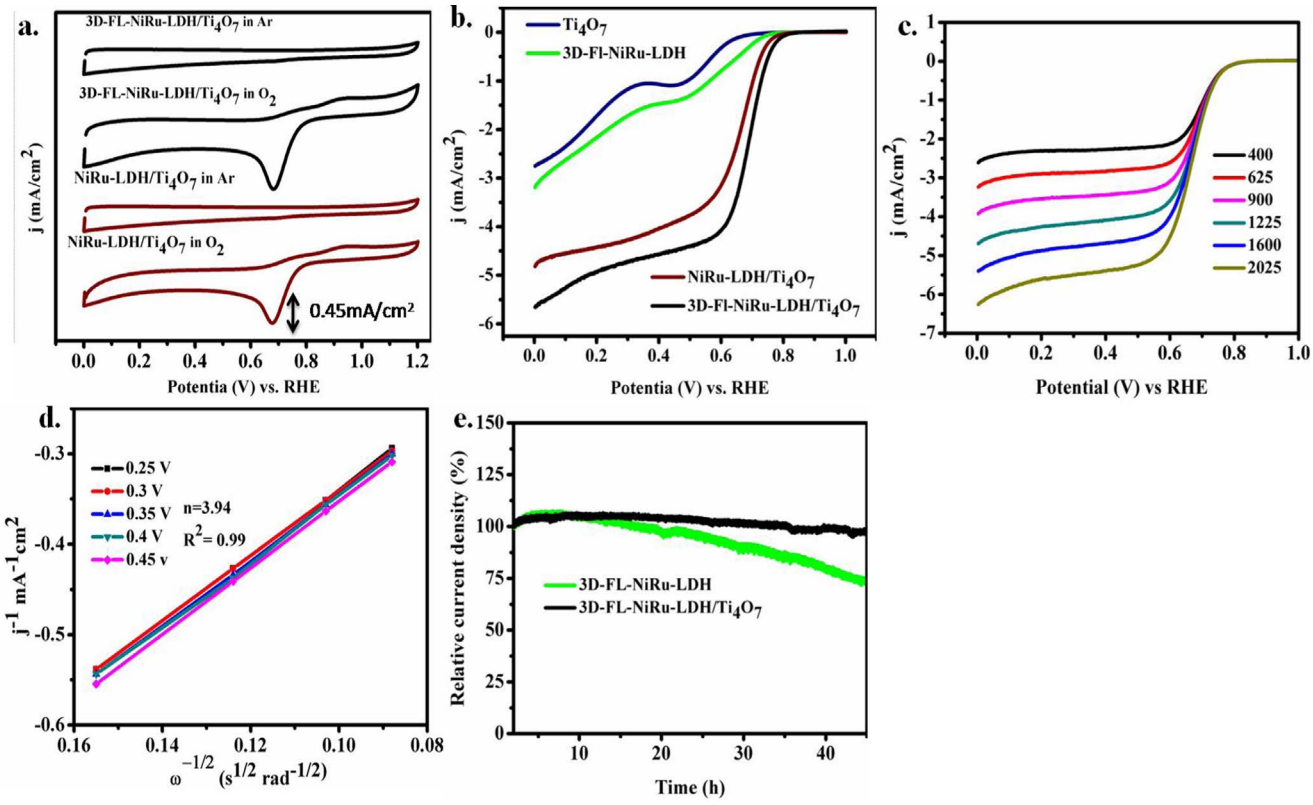

Fig. 4. Measurement of ORR activity for NiRu-LDHs. (a) CV curves for 3D-FL-NiRu-LDH/Ti_4O_7 and NiRu-LDH/Ti_4O_7 in Ar and O_2-saturated electrolyte. (b) ORR polarization curves of 3D-FL-NiRu-LDH, Ti_4O_7, 3D-FL-NiRu-LDH/Ti_4O_7, and NiRu-LDH/Ti_4O_7 at a rotation rate of 1600 rpm and a scan rate of 1 mV s^{-1}. (c) ORR polarization curves of 3D-FL-NiRu-LDH/Ti_4O_7 at different rotation rates (400, 625, 900, 1225, 1600, 2025 rpm). (d) The corresponding K-L plots, which represent the high selectivity of the 3D-FL-NiRu-LDH/Ti_4O_7 catalyst (e). ORR stability test for 3D-FL-NiRu-LDH, 3D-FL-NiRu-LDH/Ti_4O_7, and 20% Pt/C under 1 M KOH.

Table 2
Summary of ORR performance and stability between 3D-FL-NiRu-LDH/Ti_4O_7 and previously reported electrocatalysts.

Material	Onset Potential (V vs RHE)	Cathodic ORR peak (V vs RHE)	Stability	Ref.
$Ni_2Co^{III}Fe$-LDH/N-GO	0.88		8 h at 10 mA cm^{-1} (85%)	[14]
$NiCo_2S_4$@N/S-rGO	0.85 V	0.72 V	20 h at 0.5 V (~ 82%)	[34]
NiFe-LDH/Fe-N-C (1:3)	0.863 V	–	24 h at −3 mA cm^{-1} (~ 76%)	[35]
O-NiCoFe-LDH	~0.8 V	~0.60 V	40 h at 0.7 V (~ 90%)	[13]
20 wt% Pt/C	1.0 V		13 h at 0.7 V (~ 95%)	This work
3D-FL-NiRu-LDH	0.7 V	–	45 h at 0.7 V (75%)	This work
3D-FL-NiRu-LDH/Ti_4O_7	~0.85 V	~0.70 V	45 h at 0.7 V (~ 98%)	This work
NiRu-LDH/Ti_4O_7	0.80	0.65	–	This work

other LDH based catalysts. In order to confirm this, a continuous chronoamperometry measurement was taken for about 45 h. Based on that, the 3D-FL-NiRu-LDH/Ti_4O_7 (Fig. 4**e**) sustains > 98%, bare 3D-FL-NiRu-LDH (75%) of activity. However, 20% Pt/C (Fig. S6f) can sustain only its 95% even after 13 h. The long term durability of 3D-FL-NiRu-LDH/Ti_4O_7 might be emanated from the deterrence of agglomeration due to strong inter coupling between the Ti_4O_7 and LDH nanosheet as evidenced in XPS and the intrinsic nature of considerable structural robustness of Ti_4O_7 that helps the LDH to retain its original structural integrity. Another important key role of Ti_4O_7 could be, capable to attract the absorption of anions, so that the intercalated carbonate ions can be shielded from the diffusive attacks of anions, so that the layered structure could be maintained, when compared with the corresponding bare catalyst [43].

In general, the superior performance of the hybrid possibly arises from several factors. **(1)** the intrinsic high activity of NiRu-LDH (Fig. 4**b**); **(2)** the high dispersion of nanocrystalline 3D-FL-NiRu-LDH **(3)** the strong coupling effect between the LDH and the robust and conductive Ti_4O_7 pillar that minimizes particle agglomeration and produce an electronic effect on LDH, as evidenced by the XPS spectra (Fig. 3**a-c**) hence, agglomeration of nanoparticles can be reduced by choosing a support which has strong interactions with the metal. **(4)** Due to morphological engineering of NiRu-LDH/Ti_4O_7 in to 3D-FL-NiRu-LDH/Ti_4O_7 that is responsible to expose extra active site and make easy of accessible electrolyte with the catalyst surface.

4. Conclusion

This is the first report to combine LDH materials with robust, conductive and stable metal oxide pillars. The 3D- FL-NiRu-LDH/Ti_4O_7 composite showed promising ORR activity, with negligible degradation in 45 h in 1 M KOH. NiRu-LDHs were purposely re-formed into three dimensional flower-like structures using a template to increase the surface area, whereby the active sites were expected to increase and also to be more accessible to the electrolyte. The addition of robust and conductive Ti_4O_7 pillars minimizes the aggregation of LDH particles and prevents the hybrid material from collapse. This uniform dispersion of two materials facilitates electron transport for oxygen

electrocatalysis, as evidence by XPS. The strong coupling effect between nanocrystalline 3D-FL-NiRu-LDHs and conductive Magneli phase Ti_4O_7 pillars, as well as the morphological modification generate a synergy for high catalytic activity and durability for the oxygen reduction reaction under alkaline conditions. Compared to commonly used carbon support, the findings could indicate a new direction to improve the durability of various commonly seen LDH materials.

Acknowledgement

Financial support was provided by the Ministry of Science and Technology (MOST) (105-3113-E-011-001, 104-2911-I-011-505-MY2, 103-2923-E-011-004-MY3), the Ministry of Economic Affairs (MOEA) (101-EC-17-A-08-S1-183) the Top University Projects of Ministry of Education (MOE) (100H451401), and Taiwan's Deep Decarbonization Pathways toward a Sustainable Society Project (106-0210-02-11-03). Research facilities were provided by the National Synchrotron Radiation Research Center (NSRRC) and the National Taiwan University of Science and Technology (NTUST). Last but not least, we would like to thanks to Prof. Cheng-Yen Wen from Department of Material science and Engineering, National Taiwan University, Taipei, 106, Taiwan for his willing to measure TEM in his laboratory and Mr. Chia-Hao Yu for helping us on operating the instrument.

Appendix A. Supporting information

Supplementary data associated with this article can be found in the online version at http://dx.doi.org/10.1016/j.nanoen.2018.03.017.

References

[1] T.R. Cook, D.K. Dogutan, S.Y. Reece, Y. Surendranath, T.S. Teets, D.G. Nocera, Chem. Rev. (Wash., DC, U.S.) 110 (2010) 6474–6502.
[2] Z. Lu, W. Zhu, X. Lei, G.R. Williams, D. O'Hare, Z. Chang, X. Sun, X. Duan, Nanoscale 4 (2012) 3640–3643.
[3] M. Latorre-Sanchez, P. Atienzar, G. Abellán, M. Puche, V. Fornés, A. Ribera, H. García, Carbon 50 (2012) 518–525.
[4] Y. Zhang, B. Cui, C. Zhao, H. Lin, J. Li, Phys. Chem. Chem. Phys. 15 (2013) 7363–7369.
[5] C. Mousty, Anal. Bioanal. Chem. 396 (2010) 315–325.
[6] F. Cavani, F. Trifirò, A. Vaccari, Catal. Today 11 (1991) 173–301.
[7] G. Fan, F. Li, D.G. Evans, X. Duan, Chem. Soc. Rev. 43 (2014) 7040–7066.
[8] X. Yu, M. Zhang, W. Yuan, G. Shi, J. Mater. Chem. A 3 (2015) 6921–6928.
[9] M. Gong, Y. Li, H. Wang, Y. Liang, J.Z. Wu, J. Zhou, J. Wang, T. Regier, F. Wei, H. Dai, J. Am. Chem. Soc. 135 (2013) 8452–8455.
[10] X. Zhu, C. Tang, H.-F. Wang, B.-Q. Li, Q. Zhang, C. Li, C. Yang, F. Wei, J. Mater. Chem. A 4 (2016) 7245–7250.
[11] F. Song, X. Hu, J. Am. Chem. Soc. 136 (2014) 16481–16484.
[12] X. Han, C. Yu, J. Yang, C. Zhao, H. Huang, Z. Liu, P.M. Ajayan, J. Qiu, Adv. Mater. Interfaces 3 (7) (2016) 1500782.
[13] S.J. Kim, Y. Lee, D.K. Lee, J.W. Lee, J.K. Kang, J. Mater. Chem. A 2 (2014) 4136–4139.
[14] X. Long, J. Li, S. Xiao, K. Yan, Z. Wang, H. Chen, S. Yang, Angew. Chem. Int. Ed. 53 (2014) 7584–7588.
[15] J. Zhao, J. Chen, S. Xu, M. Shao, Q. Zhang, F. Wei, J. Ma, M. Wei, D.G. Evans, X. Duan, Adv. Funct. Mater. 24 (2014) 2938–2946.
[16] Y. Zhao, B. Li, Q. Wang, W. Gao, C.J. Wang, M. Wei, D.G. Evans, X. Duan, D. O'Hare, Chem. Sci. 5 (2014) 951–958.
[17] L. Qian, Z. Lu, T. Xu, X. Wu, Y. Tian, Y. Li, Z. Huo, X. Sun, X. Duan, Adv. Energy. 5 (2015) (1500245-n/a).
[18] Y. Zhao, P. Chen, B. Zhang, D.S. Su, S. Zhang, L. Tian, J. Lu, Z. Li, X. Cao, B. Wang, M. Wei, D.G. Evans, X. Duan, Chem. – Eur. J. 18 (2012) 11949–11958.
[19] B. Li, Y. Zhao, S. Zhang, W. Gao, M. Wei, ACS Appl. Mater. Interfaces 5 (2013) 10233–10239.
[20] D. Zhou, Z. Cai, X. Lei, W. Tian, Y. Bi, Y. Jia, N. Han, T. Gao, Q. Zhang, Y. Kuang, J. Pan, X. Sun, X. Duan, Adv. Energy Mater. (2017) 1701905, http://dx.doi.org/10.1002/aenm.201701905.
[21] C. Tang, H.-F. Wang, X.-L. Zhu, B.-Q. Li, Q. Zhang, Part. Part. Syst. Charact. 33 (2016) 473–486.
[22] J.-X. Feng, H. Xu, Y.-T. Dong, S.-H. Ye, Y.-X. Tong, G.-R. Li, Angew. Chem. Int. Ed. 55 (2016) 3694–3698.
[23] C. Yao, F. Li, X. Li, D. Xia, J. Mater. Chem. 22 (2012) 16560–16565.
[24] V.T.T. Ho, C.-J. Pan, J. Rick, W.-N. Su, B.-J. Hwang, J. Am. Chem. Soc. 133 (2011) 11716–11724.
[25] B.-J. Hsieh, M.-C. Tsai, C.-J. Pan, W.-N. Su, J. Rick, H.-L. Chou, J.-F. Lee, B.-J. Hwang, Electrochim. Acta 224 (2017) 452–459.
[26] S.J. Tauster, S.C. Fung, R.L. Garten, J. Am. Chem. Soc. 100 (1978) 170–175.
[27] C.-J. Pan, M.-C. Tsai, W.-N. Su, J. Rick, N.G. Akalework, A.K. Agegnehu, S.-Y. Cheng, B.-J. Hwang, J. Taiwan Inst. Chem. Eng. 74 (2017) 154–186.
[28] N.-L. Wu, S.-Y. Wang, I.A. Rusakova, Science (New York, N.Y.) 285 (1999) 1375–1377.
[29] Y. Dou, S. Zhang, T. Pan, S. Xu, A. Zhou, M. Pu, H. Yan, J. Han, M. Wei, D.G. Evans, X. Duan, Adv. Funct. Mater. 25 (2015) 2243–2249.
[30] J. Luo, J.-H. Im, M.T. Mayer, M. Schreier, M.K. Nazeeruddin, N.-G. Park, S.D. Tilley, H.J. Fan, M. Grätzel, Science 345 (2014) 1593–1596.
[31] C. Luo, D. Li, W. Wu, Y. Zhang, C. Pan, RSC Adv. 4 (2014) 3090–3095.
[32] W.L. Kwong, C.C. Lee, J. Messinger, J. Phys. Chem. C 120 (2016) 10941–10950.
[33] J. Jiang, C. Zhang, L. Ai, Electrochim. Acta 208 (2016) 17–24.
[34] M. Mora, C. Jiménez-Sanchidrián, J. Rafael Ruiz, Mater. Lett. 120 (2014) 193–195.
[35] S. Nayak, L. Mohapatra, K. Parida, J. Mater. Chem. A 3 (2015) 18622–18635.
[36] E. Alibakhshi, E. Ghasemi, M. Mahdavian, B. Ramezanzadeh, S. Farashi, J. Electrochem. Soc. 163 (2016) C495–C505.
[37] M.N. Sepehr, T.J. Al-Musawi, E. Ghahramani, H. Kazemian, M. Zarrabi, Arab. J. Chem. 10 (2017) 611–623.
[38] L. Wang, X. Xu, D.G. Evans, X. Duan, D. Li, J. Solid State Chem. 183 (2010) 1114–1119.
[39] Y. Zhang, H. Jiang, G. Li, M. Zhang, RSC Adv. 6 (2016) 16851–16858.
[40] K. Yamaguchi, T. Koike, J.W. Kim, Y. Ogasawara, N. Mizuno, Chem. – Eur. J. 14 (2008) 11480–11487.
[41] S. Wu, L. Chen, B. Yin, Y. Li, Chem. Commun. (Camb., U.K.) 51 (2015) 9884–9887.
[42] G. Wang, L. Xiao, B. Huang, Z. Ren, X. Tang, L. Zhuang, J. Lu, J. Mater. Chem. 22 (2012) 15769–15774.
[43] Z. Chang, N. Zhao, J. Liu, F. Li, D.G. Evans, X. Duan, C. Forano, M. de Roy, J. Solid State Chem. 184 (2011) 3232–3239.